


Article

Coupling of Soil Moisture and Air Temperature from Multiyear Data During 1980–2013 over China

Qing Yuan, Guojie Wang *, Chenxia Zhu, Dan Lou, Daniel Fiifi Tawia Hagan , Xiaowen Ma and Mingyue Zhan

Collaborative Innovation Center on Forecast and Evaluation of Meteorological Disasters, School of Geographical Sciences, Nanjing University of Information Science & Technology, Nanjing 210044, China; qyuan@nuist.edu.cn (Q.Y.); zhuchenxia@nuist.edu.cn (C.Z.); loudan711@163.com (D.L.); dhagan@yeah.net (D.F.T.H.); 17853462199@163.com (X.M.); zhanmingyue0614@163.com (M.Z.)

* Correspondence: gwang@nuist.edu.cn; Tel.: +86-25-58731418

Received: 28 November 2019; Accepted: 24 December 2019; Published: 26 December 2019



Abstract: Soil moisture is an important parameter in land surface processes, which can control the surface energy and water budgets and thus affect the air temperature. Studying the coupling between soil moisture and air temperature is of vital importance for forecasting climate change. This study evaluates this coupling over China from 1980–2013 by using an energy-based diagnostic method, which represents the momentum, heat, and water conservation equations in the atmosphere, while the contributions of soil moisture are treated as external forcing. The results showed that the soil moisture–temperature coupling is strongest in the transitional climate zones between wet and dry climates, which here includes Northeast China and part of the Tibetan Plateau from a viewpoint of annual average. Furthermore, the soil moisture–temperature coupling was found to be stronger in spring than in the other seasons over China, and over different typical climatic zones, it also varied greatly in different seasons. We conducted two case studies (the heatwaves of 2013 in Southeast China and 2009 in North China) to understand the impact of soil moisture–temperature coupling during heatwaves. The results indicated that over areas with soil moisture deficit and temperature anomalies, the coupling strength intensified. This suggests that soil moisture deficits could lead to enhanced heat anomalies, and thus, result in enhanced soil moisture coupling with temperature. This demonstrates the importance of soil moisture and the need to thoroughly study it and its role within the land–atmosphere interaction and the climate on the whole.

Keywords: soil moisture–temperature coupling; heatwaves; multiple time scales

1. Introduction

The summer of 2013 was unprecedentedly hot in Eastern China, causing substantial societal and economic impacts [1]. Such a phenomenon has drawn widespread concerns, and the physical mechanism behind such heatwave is gradually being discovered [2–4]. The changes of large-scale atmospheric circulations may be the main cause of temperature anomalies, and small-scale physical processes of local energy balance such as soil moisture–atmosphere coupling could also make a contribution to them [5]. Many studies have shown that soil moisture anomalies play an important role in soil moisture–temperature coupling [6,7], as it could control the energy budget by the partitioning of latent heat flux and sensible heat flux, further impacting the air temperature [8,9]. When soil moisture decreases, less water can be used for evapotranspiration, resulting in a decrease of latent heat flux [8,10]. Based on the energy balance, the decline of latent heat flux causes an increase of the sensible heat flux, thus enhancing the air temperature. These conditions indicate a negative feedback between soil moisture and air temperature: Soil moisture deficit results in the rise of air temperature [11–13].

Nowadays, various studies have shown that dry soil moisture conditions can have a substantial influence on the severity of heat waves and drought through the coupling between soil moisture and atmosphere [10,11]. As shown, soil moisture–temperature coupling helps to explain heat waves in summer climate [14,15]. Modeling experiments have focused on identifying the strong coupling regions, and how these regions are influenced by the changing climate [14,16]. The Global Land–Atmosphere Coupling (GLACE) project indicated that the strongest coupling regions (hot spots) of soil moisture–temperature are between the transitional regions of wet and dry climates [16,17]. In addition, some numerical experiments have been devoted to studying the soil moisture–temperature coupling at regional scales [18–20] finding that soil moisture anomalies impact air temperature during summer mainly in areas like Northern China [21–23].

At present, many studies have tried to use different metrics for assessing land–atmosphere coupling strengths. Koster et al. [16] proposed to use correlation between evapotranspiration and temperature, and found results agreeing with other metrics, for example, those based on the correlation between evapotranspiration and radiation. Gallego-Elvira et al. [24] used the dependence of the surface heating rate of different cover types on the previous precipitation during drought to identify different evaporative regions. Dirmeyer [25] devoted an index of surface flux sensitivity to soil moisture variability and applied it to global atmospheric reanalysis datasets. However, most studies assessing the coupling of soil moisture to climate were based primarily on summer (June–July–August, JJA) [9,14], but there is a lack of understanding on its seasonal changes; therefore, it is important to devote more attention to studying the coupling within the other seasons as well. Moreover, the studies of the soil moisture–temperature coupling were mostly based on modeling experiments [10,26], which show a large difference in the regions and strengths of land–atmosphere coupling [8]. However, the limited ground measurements of soil moisture cannot meet the research needs of land–atmosphere coupling on regional scales. Given the limitation of ground measurements, satellite data could be used in soil moisture–temperature coupling studies from an observational point of view, and the recent development of soil moisture and evapotranspiration products from remote sensing technology provides the possibility for such studies.

A wide variety of datasets makes it possible for us to study soil moisture–temperature coupling from an observational perspective [24,27,28]. This study utilized one of these satellite-based datasets with a coupling diagnostic to show the spatial distribution and interannual variation of strong coupling regimes between soil moisture and temperature over China in different seasons. This diagnostic focused on two different timescales to fill the gap between extremes and climatological studies of soil moisture–temperature coupling. Different season coupling hot spots of China are illustrated in the following sections. Subsequently, we explored the role of soil moisture during the 2013 heatwave in Southeast China and the 2009 event in North China.

Furthermore, this study depicts not only soil moisture–temperature coupling in long-term variations, but also soil moisture–temperature coupling during the heat wave events and the related heating processes. It may help to point us toward better understanding the underlying processes of soil moisture–temperature coupling, and thus improve the prediction skills of heat waves [14,29].

2. Materials and Methods

2.1. Study Area

China has a complex climate due to its topography [30]. Mainland China is generally divided into three different climatic zones: Arid region with annual precipitation below 200 mm, humid region with annual precipitation more than 800 mm, and transitional region with annual precipitation from 200 to 800 mm [31]. The arid region mainly includes Xinjiang province and western Inner Mongolia Plateau. The humid region is mainly South China. The transitional region mainly includes North China Plain, Northeast Plain, and part of Tibetan Plateau, where there is more rain in summer but less in winter. Known as the “The Third Pole”, the Tibetan Plateau is the highest and most unique

geographical unit on earth [32]. It is one of the most sensitive regions to global climate change and its hydrological processes are quite different from that of other regions of China [33,34]; thus, it is regarded as a separate typical region in this study. The humid, transitional, and dry regions, as well as the Tibetan Plateau, are shown in Figure 1.

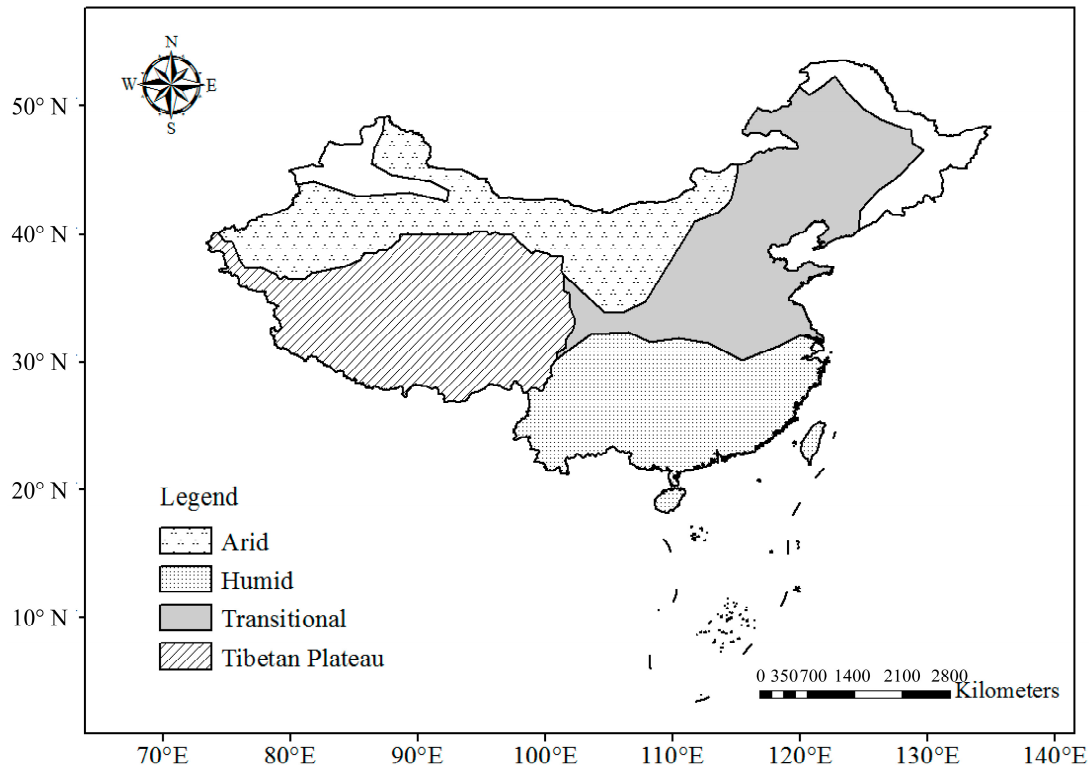


Figure 1. The typical climate regions of China (arid, humid, transitional, the Tibetan Plateau).

2.2. Data Sources

The evapotranspiration (ET) and potential evapotranspiration (PET) data from the GLEAM v3.0a (Global Land Evaporation Amsterdam Model) product were used in this study, which span the period from 1980 to 2015 with a spatial resolution of 0.25° . The GLEAM model is a simplified land model, which is fully dedicated to estimating the terrestrial evaporation and root zone soil moisture based on satellite data [35]. It comprises a set of algorithms using multiyear satellite observations to estimate the components of terrestrial ET. The PET is calculated within the Priestley–Taylor equation via the observations of net radiation and near-surface air temperature [36]. The 2-m air temperature and the top layer (0–7 cm) volumetric soil moisture from the ERA-Interim reanalysis data were used [37].

2.3. Methods

This study used a diagnostic method to estimate the long-term soil moisture–temperature coupling over China in different seasons, which is based on two energy balances of ET and PET. The partitioning of the land energy is expressed in Equation (1), where R_n refers to the surface net radiation, G means the ground heat flux, and λ is the latent heat of vaporization, which can be captured from near-surface air temperature; the ground heat flux is negligible in this study [36,38].

$$R_n - G = \lambda E + H, \quad (1)$$

When the annual time series of E , E_p , R_n , and near-surface temperature (T) are available, the diagnostic method could be used to estimate the long-term soil moisture–temperature coupling [17], where the metric (II) can be calculated as:

$$\Pi = \rho(H, T) - \rho(H_p, T), \quad (2)$$

$$H = R_n - \lambda E, \quad (3)$$

$$H_p = R_n - \lambda E_p, \quad (4)$$

where ρ means Pearson's correlation coefficient, and H is the sensible heat flux. Using Π , we can derive an indicator of the long-term soil moisture–temperature coupling, which can be considered as a multi-year average. When considering the σ_T , σ_H , and σ_{H_p} (the standard deviations of T , H , and H_p), Equation (1) could also be expressed in another form as covariances:

$$\Pi = \frac{1}{\sigma_T} \left(\frac{\text{cov}(H, T)}{\sigma_H} - \frac{\text{cov}(H_p, T)}{\sigma_{H_p}} \right), \quad (5)$$

To understand the related heating processes between land and atmosphere during the heatwave events, we used a different diagnostic method based on daily data to derive the soil moisture–temperature coupling at daily scale [8], and the metric (π) is defined as:

$$\pi_i = \frac{T_i - \bar{T}}{\sigma_T} \left(\frac{H_i - \bar{H}}{\sigma_H} - \frac{H_{p,i} - \bar{H}_p}{\sigma_{H_p}} \right), \quad (6)$$

where \bar{T} , \bar{H} , and \bar{H}_p indicate the averages of T , H , and H_p over a long term. It can be simplified as:

$$\pi = T' \times e', \quad (7)$$

$$e' = (R_n - \lambda E)' - (R_n - \lambda E_p)', \quad (8)$$

where T' represents the anomalies of T , and e' is equal to $H' - H_p'$ and indicates the contribution of soil moisture deficit to sensible heat flux. When there is sufficient soil moisture for the atmospheric demand, this energy term will be zero, and it may increase under arid condition. Only if the potential influence of soil moisture on temperature is accompanied by a large anomalous value of temperature is the local energy balance likely to control air temperature [11].

The Π and the π are two coupling metrics at different time scales; the former includes the long-term record in terms of correlation coefficients to evaluate long-term climatology, while the latter expresses anomalies of one day in terms of standard deviations to evaluate daily extreme. When Π and π values are greater than zero, then the higher the value the stronger soil moisture–temperature coupling. If values are less than or equal to zero, there is no coupling [17].

3. Results

3.1. Long-Term Soil Moisture–Temperature Coupling

To know the spatial distribution of strong coupling between soil moisture and temperature in China, we first calculated the metric (Π) by using ET (evapotranspiration) and PET (potential evapotranspiration) from the GLEAM data, and T (2-meter temperature) and R_n (surface net radiation) from the ERA-Interim reanalysis data over the period 1980–2013. Figure 2 illustrates the derived long-term soil moisture–temperature coupling annually and in different seasons.

Figure 2a shows the Π values derived from the annual data. The coupling strength appears to be highest in Northeast China and part of the Tibetan Plateau, where the climate is neither too wet nor too dry, showing that soil moisture has the strongest impact on temperature over the annual average in these regions. The results are consistent with previous studies which have suggested that such hot spots of soil moisture–temperature coupling occur most in transitional regions between wet and dry climate [9,39,40]. In spring, there appears to be strong soil moisture–temperature coupling

(Figure 2b) in large areas of China, including Northeast, North, Northwest China and the Tibetan Plateau, and Yunnan province as well.

In summer, the coupling strengths are largely reduced compared to those in spring. There are only coupling signals in North China, especially Inner Mongolia. In autumn, the strongest coupling signals appear in Northeast China and the northern part of the Tibetan Plateau, although these are also significantly weakened compared to those in spring. It is not surprising to find strong signals in Northeast China, where it is neither too wet nor too dry in summer. In the cold season of winter, quite limited coupling signals are found, indicating that the soil moisture generally has quite limited impact on temperature across China.

Over the whole region, as shown in Figure 2, soil moisture–temperature coupling is relatively stronger in spring, followed by summer and autumn, and rather insignificant in winter. The seasonality of the soil moisture–temperature coupling strength has a distinct regional variation. Over Northern China, which is mainly a arid/semi-arid region, the contribution of soil moisture to evapotranspiration is mainly limited by water. Here, the results in Figure 2 depict strong coupling, which suggests a stronger impact of soil moisture anomalies on temperature. Given that Southern China is mainly a humid/semi-humid region, the comparatively weaker soil moisture–temperature coupling (as seen in Figure 2) demonstrates that the region is mostly dominated by energy-limited conditions [8,13]. The north of China is here identified as a hot spot in spring, mainly because dry conditions (water-limited) persist throughout the year. In spring, a sufficient energy supply for ET, due to melting ice and snow, increases the amount of water in these regions, as well as causes more evaporation and, thus, increased coupling strength to the atmosphere. This may explain why coupling strength is higher in spring than in summer in North China [41]. The seasonal transition from winter to spring affects the soil moisture thawing and radiation budget over the Tibetan Plateau, which results in more heat transfer into the atmosphere. The heat energy transferred to the atmosphere is used to warm the air, thus showing strong soil moisture–temperature coupling [42]. In Yunnan province, the water supply is not sustainable because of the special climatic conditions, thus the soil is drier during the spring, which leads to a strong soil moisture–temperature coupling [43].

Figure 3 shows the soil moisture–temperature coupling strengths in different seasons based on the four climatic regions. Obviously, the coupling strengths vary greatly in different regions and different seasons. Except for the humid region, the coupling strengths of the other three climatic regions are all the strongest in spring and the weakest in winter. From the perspective of different seasons, the strength differences between the arid region, the transitional region, and the Tibetan Plateau region are relatively small. The seasonal transition from winter to spring influences soil moisture thawing and radiation budgets, with more heat energy being transferred into atmosphere [42,43]. For the typical climate regions divided according to Figure 1, the arid and transitional regions and the Tibetan Plateau zone have analogous soil moisture and atmosphere conditions, thus they are very similar, particularly in spring. However, coupling strengths in the humid region appear to be much smaller than the other regions in all seasons. The transitional region appears to have the strongest coupling strength in terms of the annual average, followed by the arid region and the Tibetan Plateau. The soil moisture–temperature coupling in spring appears to be much stronger than in the other seasons, which is particularly significant in the arid and transitional regions and the Tibetan Plateau. In the cold winter, the soil moisture–temperature coupling strengths are rather weak in all of the four climatic regions. Despite notable differences in the soil moisture–temperature coupling strengths among the four seasons, there are still some features in common. There appears to be hot spots of soil moisture–temperature coupling in the transitional zones between wet and dry regimes in all seasons.

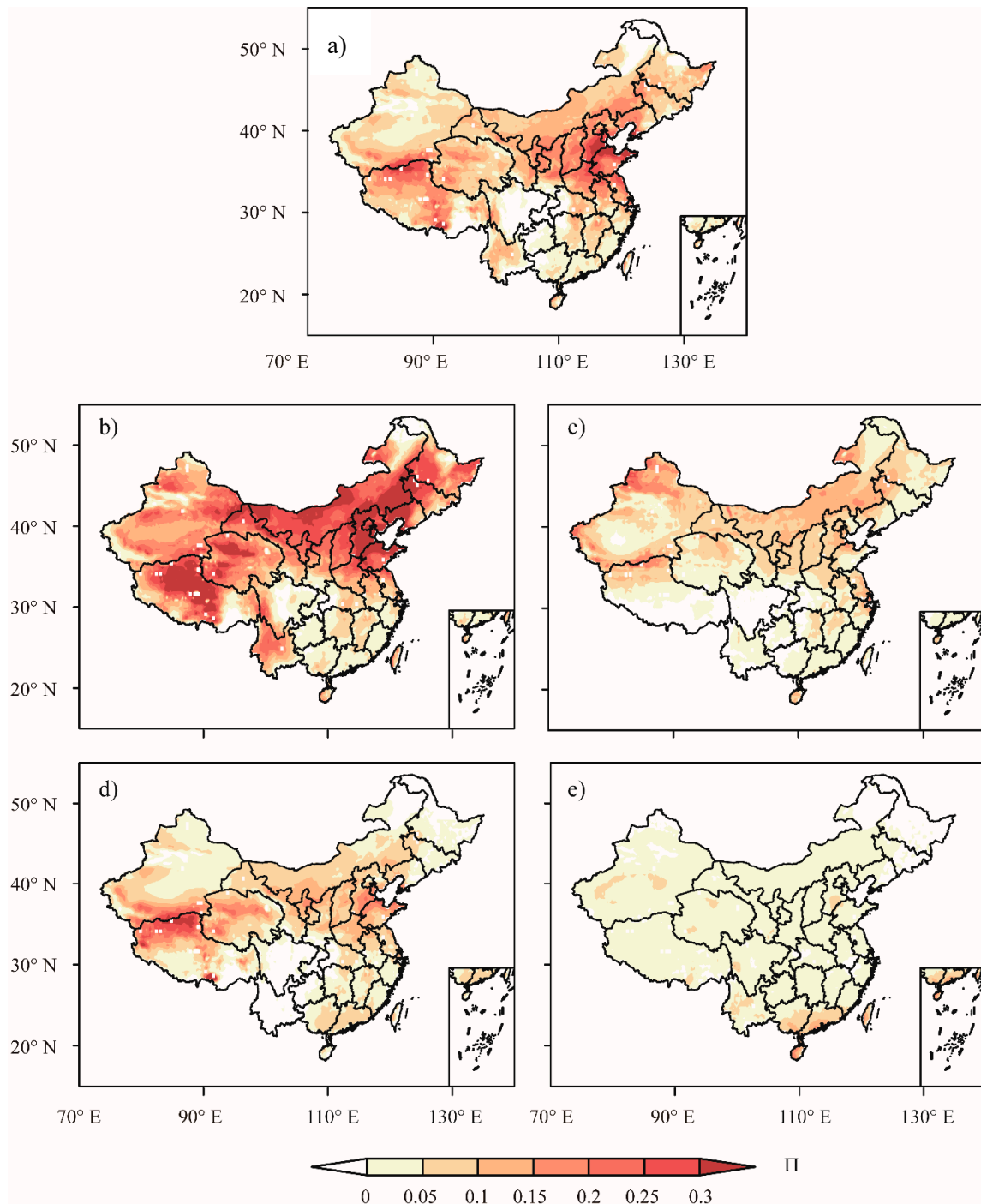


Figure 2. Soil moisture–temperature coupling over China during the period 1980–2013. (a) Whole year; (b) spring (MAM, from March to May); (c) summer (JJA, from June to August); (d) autumn (SON, from September to November); (e) winter (DJF, from December to February).

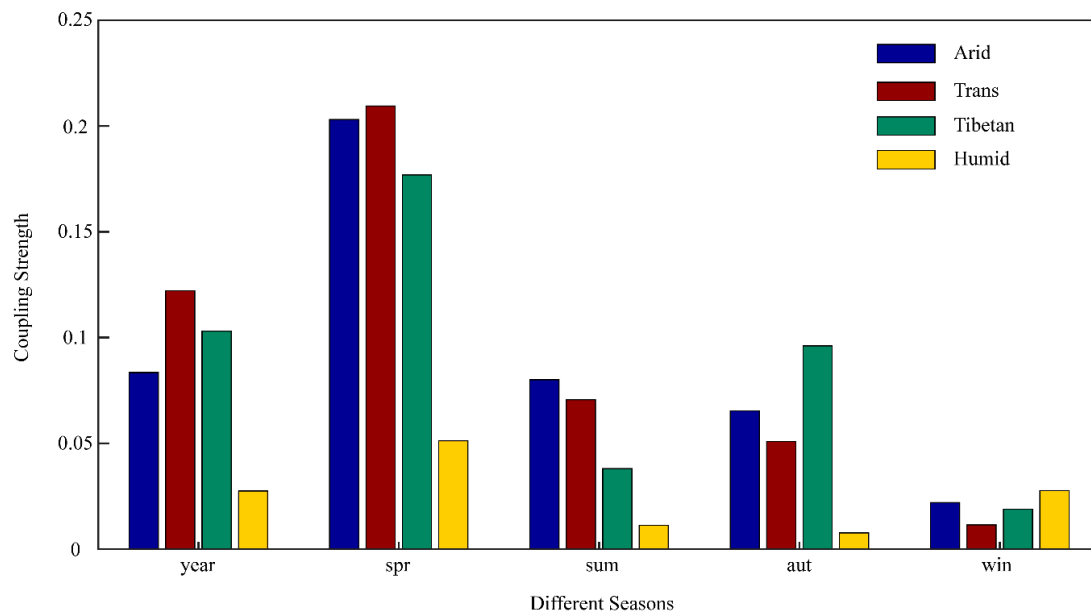


Figure 3. Soil moisture–temperature coupling strengths in different seasons in the typical climate regions over China during the period 1980–2013.

In order to understand how the soil moisture–temperature coupling strengths are linked to the soil moisture amount, Figure 4 shows the density scatter plot of coupling strengths against the soil moisture amount in spring. It appears that, principally, the coupling strengths are linearly related to the soil moisture amounts across China; when soil increases, the strength of soil moisture-temperature coupling decreases, and this linear relationship is particularly clear when the soil moisture amount is more than $0.2 \text{ m}^3/\text{m}^3$. When soil is too dry, the coupling is not sensitive to soil moisture amount, and where there is too much soil moisture, especially in the humid regions, the density of data points is also high and shows that the coupling strengths are rather low. This result is also consistent with other studies [11,13].

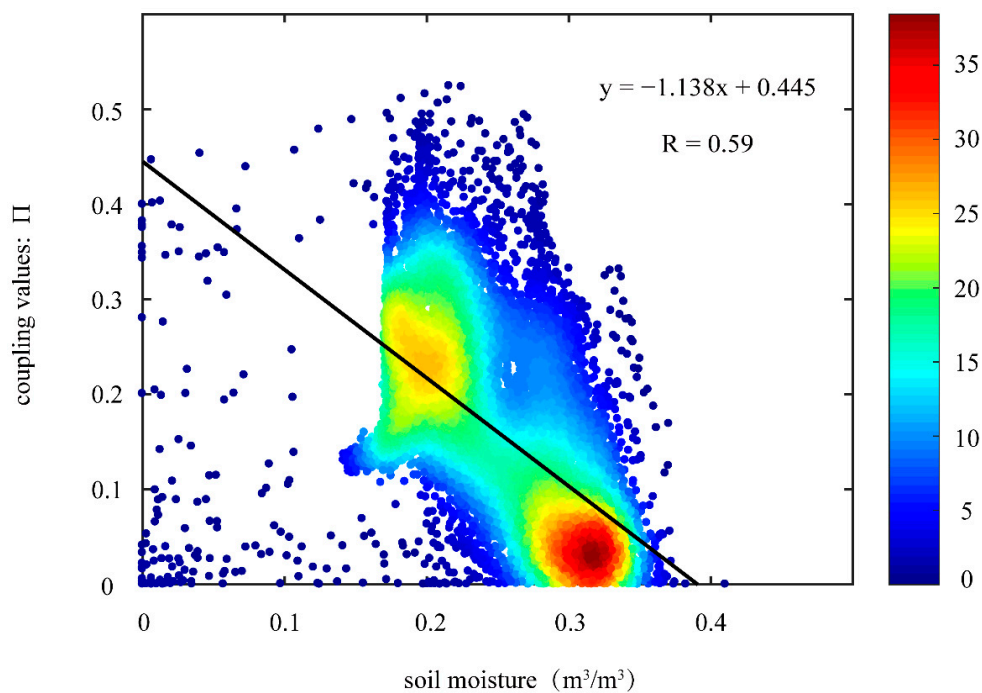


Figure 4. The density scatter plot of coupling strengths against the soil moisture amount in spring.

3.2. Coupling Anomalies in Heatwaves

As seen in Figure 2, the soil moisture–temperature coupling is strongest in spring than in other seasons in China; however, many studies have reported heat wave amplifications through the feedback loops between soil moisture deficit and temperature in summer [18,44]. To understand the detailed processes of soil moisture–temperature coupling in the heatwave events, we conducted two case studies on daily scales.

3.2.1. Case 1: Heatwave of Southeast China in Summer 2013

In the summer of 2013, Southeast China experienced abnormally high temperatures, which broke the heat records for the past 141 years and led to an unprecedented heatwave across China [1]. This unprecedented anomalies reached high values from 23 July to 14 August [3]. This disaster caused about US\$10 billion in crop damage, and a total of 5758 Heatwave-related illness cases were reported [40–47].

Figure 5a illustrates the soil moisture–temperature coupling from 1 June to 30 August, when the heatwave occurred. Figure 5b,c shows the soil moisture and temperature anomalies, referring to the multi-year average of 1980–2013. It appears that the summer temperature was strongly coupled to land surface soil moisture in East China, where the heatwave occurred. Meanwhile, there were significant soil moisture deficits and large-scale positive temperature anomalies, reaching roughly 6 °C, particularly in the middle and lower reaches of the Yangtze River basin. Atmospheric circulation anomalies are generally considered to be the main cause of heatwaves in China, e.g., the movement of the Northwest Pacific subtropical high [46,48,49]. However, land surface feedback on the atmosphere have been found to be an important factor for heatwaves over China, which may contribute 30–70% of the high temperature anomalies [22]. Our finding from Figure 5a–c is very likely to tell such a story that soil moisture deficit resulted in, at least partly, a significant heatwave through the coupled processes between land and atmosphere.

To better understand the temporal evolution of the heat wave, we show in Figure 5d–f the changes of the temperature anomalies (T') and the heat anomalies ($H' - H_p'$) with time. Figure 5d shows the positive heat anomalies before the heatwave occurred (12–23 July) in Southern China, which are related to the soil moisture deficit and lead to enhanced evaporative stress. Figure 5e illustrates the mega-heatwave from 24 July to 16 August in Southern China, when both the temperature anomalies (T') and the heat anomalies ($H' - H_p'$) reached their maximum values with the largest spatial coverage. Figure 5f shows the temperature anomalies (T') and the heat anomalies ($H' - H_p'$) during 17–28 August, when the heatwave had almost vanished with largely reduced temperature and heat anomalies, as well as their spatial coverages. Further, in Figure 5g, we show the temporal variations of ($H' - H_p'$) and T' from 1 June to 13 August, which are averaged within a small region in the epicenter of the heatwave (marked in Figure 5e). The right Y-axis indicates the metric π , and the left Y-axis indicates the anomalies of ($H' - H_p'$) and T' . It clearly shows how soil moisture deficit contributed to the enhancement of heat and temperature anomalies; it is obvious that the land–atmosphere coupling was strongest with the largest π values during the mega heatwave (23 July–18 August).

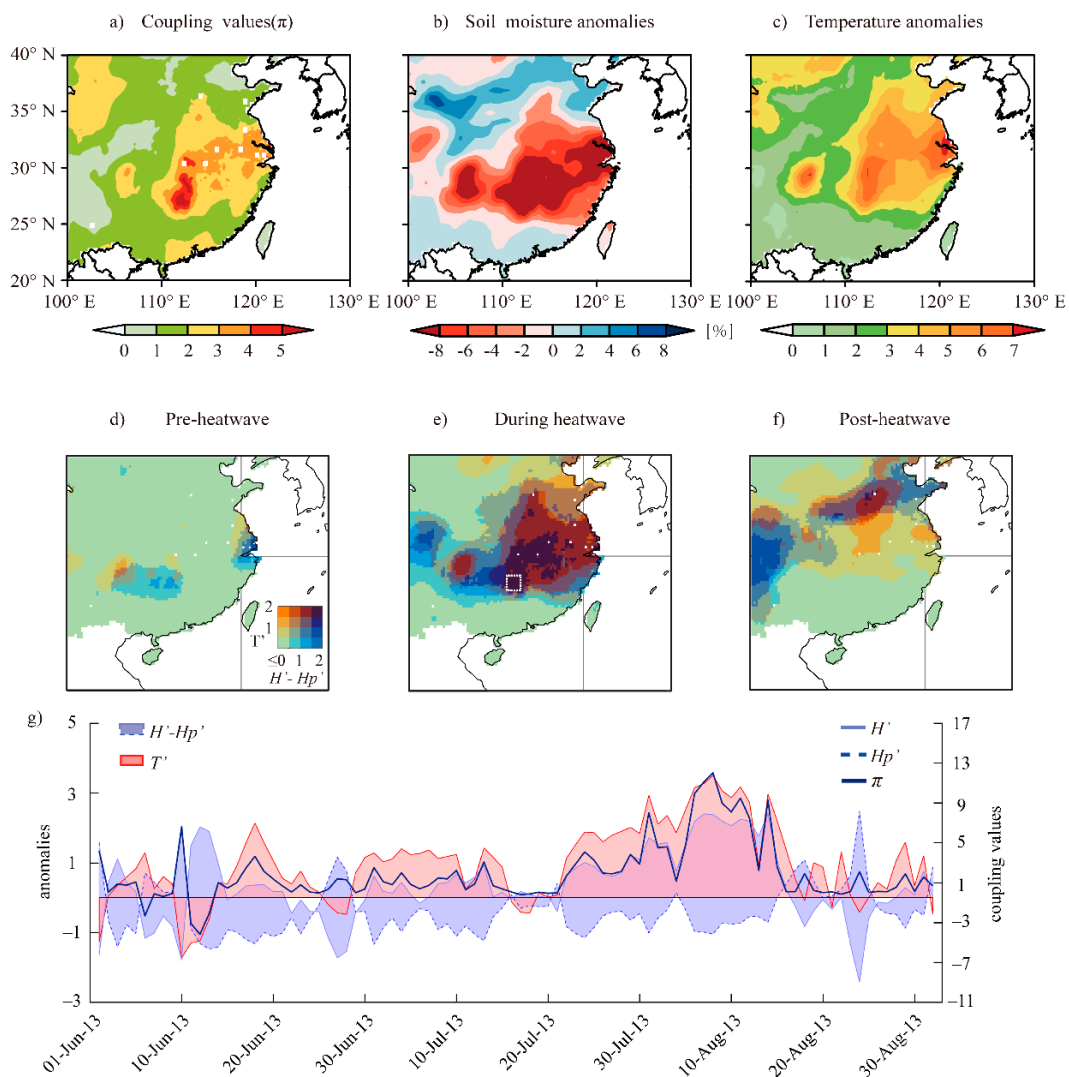


Figure 5. The soil moisture–temperature coupling and related processes during the summer heatwave of Southeast China during 24 July–16 August 2013. (a) The coupling metric π ; (b) the soil moisture anomalies and (c) the temperature anomalies, referring to the multi-year average of 1980–2013; (d) pre-heatwave (12–23 July); (e) the occurrence of the heatwave (24 July–16 August); (f) the days after the heatwave (17–28 August); (g) daily time series of T' , H' , H_p' , and the coupling metric π .

3.2.2. Case 2: Heatwave of North China in Summer 2009

There was a heatwave from 20 June to 4 July in 2009 in North China. Although it was not as severe as the mega-heatwave in Southeast China in 2013, the continuous hot weather in the North China plain was rare since 1949 [50]. At the end of June, an unprecedented heatwave hit Hebei and Shandong provinces, setting new temperature records. By early July, the heatwave gradually dissipated in North China and the high temperature shifted to Southern China [51]. The cause analysis of this event mainly focused on the effect of El Niño and is typical of the high-pressure systems [49]. In addition, the soil moisture deficit of North China would increase the sensible heat flux and influence the atmospheric boundary layer temperature, conducive to strengthening the subtropical high and causing a heatwave [52]. Figure 6a–c depicts the coupling metric π , as well as the soil moisture and temperature anomalies referring to multi-year average of 1980–2013 during the heatwave (20 June–4 July) in North China in 2009. Where there is the strongest coupling, there is significant soil moisture deficit and maximum temperature anomalies.

Figure 6d–f is analogous to Figure 5d–f, dividing the study period into pre-heatwave (the left panel), the mega heatwave (the middle panel), and post-heatwave (the right panel). It appears that the heat anomalies ($H' - H_p'$) and the temperature anomalies (T') reached their maximum values during the heatwave, while such anomalies existed in neither the left nor the right panel. In Figure 6f, we show ($H' - H_p'$) and T' for the period 1 June–31 August, averaged within a small region in the epicenter of the heatwave (marked in Figure 6e). Similarly, it is obvious that the land–atmosphere coupling is strongest with the largest π values during the mega heatwave 20 during June to 4 July, when there is the largest heat and temperature anomalies associated with a significant soil moisture deficit.

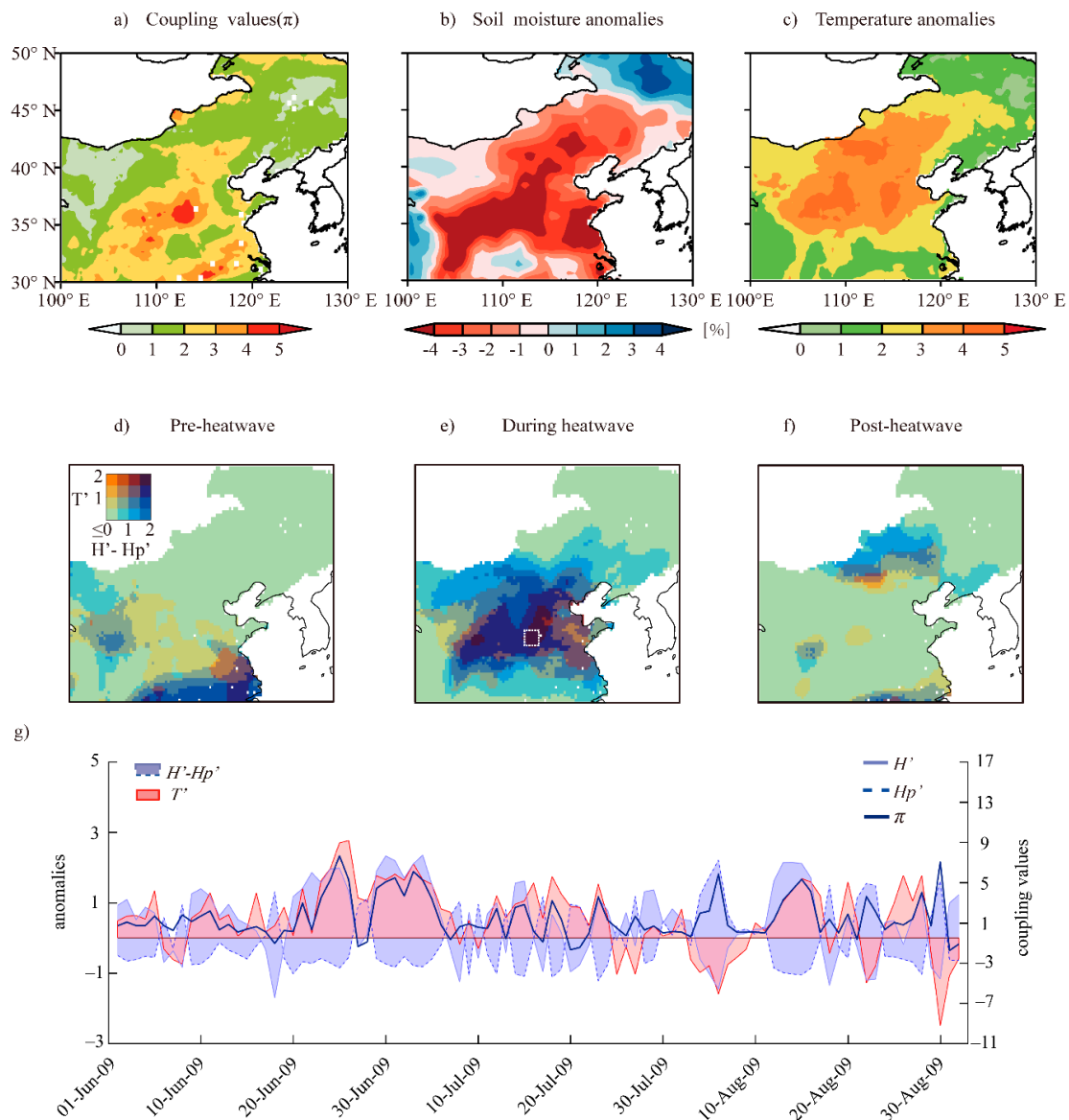


Figure 6. The soil moisture–temperature coupling and related processes during the summer heatwave of North China during 20 June–4 July 2009. (a) The coupling metric π ; (b) the soil moisture anomalies and (c) the temperature anomalies referring to the multi-year average of 1980–2013; (d) pre-heatwave (12–19 June); (e) the occurrence of the heatwave (20 June–5 July); (f) the days after the heatwave (6–13 July); (g) daily time series of T' , H' , H_p' , and the coupling metric π .

4. Conclusions and Discussion

This study attempted to utilize the GELAM and ERA-Interim datasets to study land–atmosphere coupling in China for the period 1980–2013. The key findings are as follows.

Hot spots of soil moisture–temperature coupling were found in North China and over the Tibetan Plateau, which indicate that the soil moisture–temperature coupling is strongest in the transitional climate zones. These results are in agreement with [9,14]. The seasonality of soil moisture–temperature coupling strength has marked regional variation, which suggests that soil moisture–temperature coupling strength is stronger in Northern China than in the southern, and coupling is relatively stronger in spring, followed by summer and autumn, and insignificant in winter. In spring, soil moisture–temperature coupling is stronger within dry areas, and these regimes are mainly water-limited regions, where evaporation depends on the supply of water.

Case studies involving the 2013 Southeast China heatwave and the 2009 North China heatwave were conducted to understand the role of soil moisture–temperature coupling and the related heating processes during heatwave events. It was found that enhanced heat and temperature anomalies associated with soil moisture deficit, when the soil moisture–temperature coupling intensifies, could result in enhanced evaporative stress and heat anomalies, which finally leads to enhanced soil moisture coupling with temperature [1,50]. However, there is much debate about the exact physical mechanisms of how heatwaves occur and evolve. Mirelles et al. [11] found that the prevailing persistent synoptic patterns led to warm air advection and clear skies, along with a high atmospheric demand, intensified soil desiccation (causing a strong surface sensible heat flux), causing the mega-heatwaves of 2003 and 2010 in Europe. Zhang et al. [53] supports that soil moisture in spring and early summer may be an important contributor to heatwaves in July via positive subtropical high anomalies. Several studies show that the formation mechanism of heatwaves is not only caused by a certain external force, but may be influenced by circulation systems, external forcing, or local effect, and soil moisture deficit may contribute directly and indirectly to all of these processes [10].

Land–atmosphere coupling involves water, energy, and chemical elements, which affect different processes in the hydrological cycle and thus play a critical role in the climate system [8]. However, in-situ observations of soil moisture and land surface fluxes are scarce and uncertain at the appropriate scale, which has caused great difficulties in the study of land–atmosphere coupling. The recent advances in satellite remote sensing have provided near-real-time datasets for us, and reanalysis data can also provide long-term databases for such studies. The long-term memory of soil moisture could help better understand the land–atmosphere interactions and may provide valuable information in weather forecasts to aid the management of extremely warm climates.

Other dynamic relations between soil moisture and atmosphere coupling were ignored in this study, which may also affect the participation of sensible heat and latent heat. Furthermore, the ultimate causal relationship was not demonstrated in the diagnostics between soil moisture and temperature coupling. The physical mechanism and causal relationship between soil moisture and temperature still need to be further explored in future work.

Author Contributions: Q.Y. and G.W. conceived and designed the overall project, and wrote most of sections of the manuscript. C.Z. and D.F.T.H. performed methodology and data analysis. D.L., X.M. and M.Z. supplied suggestions and comments for the manuscript. All authors have read and agreed the published version of the manuscript.

Funding: This study was funded by the National Natural Science Foundation of China (41875094, 41850410492).

Acknowledgments: All authors are grateful to the anonymous reviewers and editors for their constructive comments on earlier versions of the manuscript.

Conflicts of Interest: The authors declare no conflict of interest.

References

1. Sun, Y.; Zhang, X.; Zwiers, F.W.; Song, L.C.; Wang, H.; Yin, H.; Ren, G.Y. Rapid increase in the risk of extreme summer heat in Eastern China. *Nat. Clim. Chang.* **2014**, *4*, 1082–1085. [[CrossRef](#)]
2. Zhu, Z. An Analysis of Drought Event and Its Causation in Jianghuai Region During Summer 2013. *J. North China Inst. Aerosp. Eng.* **2016**, *26*, 37–40.

3. Gong, Z.Q.; Wang, Y.J.; Wang, Z.Y.; Ma, L.J.; Sun, C.H.; Zhang, S.Q. Briefly Analysis on Climate Anomalies and Causations in Summer 2013. *Meteorol. Mon.* **2014**, *40*, 119–125.
4. Xia, Y.; Xu, H.M. Circulation characteristics and causes of the summer extreme high temperature event in the middle and lower reaches of the Yangtze River of 2013. *J. Meteorol. Sci.* **2017**, *37*, 60–69.
5. Jaeger, E.B.; Seneviratne, S.I. Impact of soil moisture-atmosphere coupling on European climate extremes and trends in a regional climate model. *Clim. Dyn.* **2011**, *36*, 1919–1939. [[CrossRef](#)]
6. Dong, J.Z.; Crow, W.T. The Added Value of Assimilating Remotely Sensed Soil Moisture for Estimating Summertime Soil Moisture–Air Temperature Coupling Strength. *Water Resour. Res.* **2018**, *54*, 6072–6084. [[CrossRef](#)]
7. Gevaert, A.I.; Miralles, D.G.; Jeu, R.A.M.; Schellekens, J.; Dolmon, A.J. Soil Moisture–Temperature Coupling in a Set of Land Surface Models. *J. Geophys. Res. Atmos.* **2017**, *123*, 1481–1498. [[CrossRef](#)]
8. Seneviratne, S.I.; Corti, T.; Davin, E.L.; Hirschi, M.; Jaeger, E.B.; Lehner, I.; Orlowsky, B.; Teuling, A.J. Investigating soil moisture–climate interactions in a changing climate: A review. *Earth-Sci. Rev.* **2010**, *99*, 125–161. [[CrossRef](#)]
9. Koster, R.D.; Dirmeyer, P.A.; Guo, Z.; Bonan, G.; Chan, E.; Cox, P.; Gordon, C.T.; Kanae, S.; Kowalczyk, E.; Lawrence, D.; et al. Regions of strong coupling between soil moisture and precipitation. *Science* **2004**, *305*, 1138–1140. [[CrossRef](#)]
10. Fischer, E.M.; Seneviratne, S.I.; Luthi, D.; Schar, C. Contribution of land–atmosphere coupling to recent European summer heat waves. *Geophys. Res. Lett.* **2007**, *34*, L06707. [[CrossRef](#)]
11. Miralles, D.G.; Teuling, A.J.; Heerwaarden, C.C.; Arellano, J.V. Mega-heatwave temperatures due to combined soil desiccation and atmospheric heat accumulation. *Nat. Geosci.* **2014**, *7*, 345–349. [[CrossRef](#)]
12. Schwingshackl, C.; Hirschi, M.; Seneviratne, S.I. Quantifying spatiotemporal variations of soil moisture control on surface energy balance and near-surface air temperature. *J. Clim.* **2017**, *30*, 7105–7124. [[CrossRef](#)]
13. Koster, R.D.; Schubert, S.D.; Suarez, M.J. Analyzing the concurrence of meteorological droughts and warm periods, with implications for the determination of evaporative regime. *J. Clim.* **2009**, *22*, 3331–3341. [[CrossRef](#)]
14. Seneviratne, S.I.; Luthi, D.; Litschi, M.; Schar, C. Land–atmosphere coupling and climate change in Europe. *Nature* **2006**, *443*, 205–209. [[CrossRef](#)]
15. Vidale, P.L.; Luthi, D.; Wegmann, R.; Schar, C. European summer climate variability in a heterogeneous multi-model ensemble. *Clim. Chang.* **2007**, *81*, 209–232. [[CrossRef](#)]
16. Koster, R.D.; Guo, Z.C.; Dirmeyer, P.A.; Bonan, G.; Chan, E.; Cox, P.; Davies, H.; Gordon, C.T.; Kowalczyk, E.; Lawrence, D.; et al. GLACE: The Global Land–Atmosphere Coupling Experiment. Part I: Overview. *J. Hydrometeorol.* **2006**, *7*, 611–625. [[CrossRef](#)]
17. Miralles, D.G.; Berg, M.J.; Teuling, A.J.; Jeu, R.A.M. Soil moisture–temperature coupling: A multiscale observational analysis. *Geophys. Res. Lett.* **2012**, *39*, 2–7. [[CrossRef](#)]
18. Seneviratne, S.I.; Wilhelm, M.; Stanelle, T.; Hurk, B.; Hagemann, S.; Berg, A.; Cheruy, F.; Higgins, M.E.; Meier, A.; Brovkin, V.; et al. Impact of soil moisture–climate feedbacks on CMIP5 projections: First results from the GLACE–CMIP5 experiment. *Geophys. Res. Lett.* **2013**, *40*, 5212–5217. [[CrossRef](#)]
19. Hirsch, A.L.; Pitman, A.J.; Seneviratne, S.I.; Evans, J.P.; Haverd, V. Summertime maximum and minimum temperature coupling asymmetry over Australia determined using WRF. *Geophys. Res. Lett.* **2014**, *41*, 1546–1552. [[CrossRef](#)]
20. Whan, K.; Zscheischler, J.; Orth, R.; Shongwe, M.; Rahimi, M.; Asare, E.O.; Seneviratne, S.I. Impact of soil moisture on extreme maximum temperatures in Europe. *Weather Clim. Extrem.* **2015**, *9*, 57–67. [[CrossRef](#)]
21. Liu, D.; Wang, G.L.; Mei, R.; Yu, Z.B.; Gu, H.H. Diagnosing the Strength of Land–Atmosphere Coupling at Subseasonal to Seasonal Time Scales in Asia. *J. Hydrometeorol.* **2013**, *15*, 320–339. [[CrossRef](#)]
22. Zhang, J.Y.; Wu, L.Y.; Dong, W.J. Land–atmosphere coupling and summer climate variability over East Asia. *J. Geophys. Res. Atmos.* **2011**, *116*, 1–14. [[CrossRef](#)]
23. Liu, D.; Yu, Z.B.; Zhang, J.Y. Diagnosing the strength of soil temperature in the land atmosphere interactions over Asia based on RegCM4 model. *Glob. Planet. Chang.* **2015**, *130*, 7–21. [[CrossRef](#)]
24. Gallego-Elvira, B.; Taylor, C.M.; Harris, P.P.; Ghent, D.; Veal, K.L.; Folwell, S.S. Global observational diagnosis of soil moisture control on the land surface energy balance. *Geophys. Res. Lett.* **2016**, *43*, 2623–2631. [[CrossRef](#)]
25. Dirmeyer, P.A. The terrestrial segment of soil moisture–climate coupling. *Geophys. Res. Lett.* **2011**, *38*, 116702. [[CrossRef](#)]

26. Teuling, A.J.; Seneviratne, S.I.; Stockli, R.; Reichstein, M.; Moors, E.; Ciais, P.; Luysaert, S.; Hurk, B.; Ammann, C.; Bernhofer, C.; et al. Contrasting response of European forest and grassland energy exchange to heatwaves. *Nat. Geosci.* **2010**, *3*, 722–727. [[CrossRef](#)]
27. Balsamo, G.; Agusti-Parareda, A.; Albergel, C.; Arduini, G.; Beljaars, A.; Bidlot, J.; Blyth, E.; Bousseres, N.; Boussetta, S.; Brown, A.; et al. Satellite and in situ observations for advancing global Earth surface modelling: A Review. *Remote Sens.* **2018**, *10*, 2038. [[CrossRef](#)]
28. Levine, P.A.; Randerson, J.T.; Swenson, S.C.; Lawrence, D.M. Evaluating the strength of the land-atmosphere moisture feedback in Earth system models using satellite observations. *Hydrol. Earth Syst. Sci.* **2016**, *20*, 4837–4856. [[CrossRef](#)]
29. Diffenbaugh, N.S.; Pal, J.S.; Giorgi, F.; Gao, X.J. Heat stress intensification in the Mediterranean climate change hotspot. *Geophys. Res. Lett.* **2007**, *34*. [[CrossRef](#)]
30. Gao, X.; Shi, Y.; Song, R.; Giorgi, F.; Wang, Y.; Zhang, D. Reduction of future monsoon precipitation over China: Comparison between a high resolution RCM simulation and the driving GCM. *Meteorol. Atmos. Phys.* **2008**, *100*, 73–86. [[CrossRef](#)]
31. Liang, Y.L.; Han, M.C.; Bai, L.; Li, M.H. Spatial-temporal distribution and variation characteristics of the agricultural climate resources over recent 30 years in China. *Agric. Res. Arid Areas* **2015**, *33*, 259–267.
32. Mao, F.; Tang, S.H.; Sun, H.; Zhang, J.H. A Study of Dynamic Change of Dry and Wet Climate Regions in the Tibetan Plateau over the Last 46 Years. *Chin. J. Atmos. Sci.* **2008**, *32*, 499–507.
33. Fan, K.K.; Zhang, Q.; Sun, P.; Song, C.Q.; Yu, H.Q.; Zhu, X.D.; Shen, Z.X. Effect of soil moisture variation on land surface air temperature over Tibetan Plateau. *Acta. Geogr. Sin.* **2019**, *74*, 1–16.
34. Cheng, G.D.; Jin, H.J. Groundwater in the permafrost regions on the qinghai-tibet plateau and it changes. *Hydrogeol. J.* **2013**, *21*, 5–23. [[CrossRef](#)]
35. Miralles, D.G.; Holmes, T.R.H.; Jeu, R.A.M.D.; Gash, J.H.; Meesters, A.G.C.A.; Dolman, A.J. Global land-surface evaporation estimated from satellite-based observations. *Hydrol. Earth Syst. Sci.* **2010**, *15*, 453–469. [[CrossRef](#)]
36. Priestley, C.H.B.; Taylor, R.J. On the assessment of surface heat flux and evaporation using large-scale parameters. *Weather Rev.* **1972**, *100*, 81–92. [[CrossRef](#)]
37. Dee, D.P.; Uppala, S.M.; Simmons, A.J.; Berrisford, P.; Poli, P.; Kobayashi, S.; Andrae, U.; Balmaseda, M.A.; Balsamo, G.; Bauer, P.; et al. The ERA-Interim reanalysis: Configuration and performance of the data assimilation system. *Q. J. R. Meteorol. Soc.* **2011**, *137*, 553–597. [[CrossRef](#)]
38. Penman, H.L. Natural evaporation from open water, bare and grass. *Proc. R. Soc. A* **1948**, *193*, 120–145.
39. Zhang, Q.; Xiao, M.Z.; Singh, V.P.; Liu, L.; Xu, C.Y. Observational evidence of summer precipitation deficit-temperature coupling in China. *J. Geophys. Res. Atmos.* **2015**, *120*, 10040–10049. [[CrossRef](#)]
40. Mueller, B.; Seneviratne, S.I. Hot days induced by precipitation deficits at the global scale. *Proc. Natl. Acad. Sci. USA* **2012**, *109*, 12398–12403. [[CrossRef](#)]
41. Li, M.M.; Ma, Z.; Gu, H.; Yang, Q.; Zhang, Z. Production of a combined land surface data set and its use to assess land-atmosphere coupling in China. *J. Geophys. Res. Atmos.* **2017**, *122*, 948–965. [[CrossRef](#)]
42. Shi, X.; Wang, Y.; Xu, X.; Shi, X.; Wang, Y.; Xu, X. Effect of mesoscale topography over the Tibetan Plateau on summer precipitation in China: A regional model study. *Geophys. Res. Lett.* **2008**, *35*. [[CrossRef](#)]
43. Wang, Z.; Yang, S.; Duan, A.; Hua, W.; Ullah, K.; Liu, S. Tibetan Plateau heating as a driver of monsoon rainfall variability in Pakistan. *Clim. Dyn.* **2018**, *52*, 6121–6130. [[CrossRef](#)]
44. Vogel, M.M.; Orth, R.; Cheruy, F.; Hagemann, S.; Lorenz, R.; Hurk, B.J.J.M.; Seneviratne, S.I. Regional amplification of projected changes in extreme temperatures strongly controlled by soil moisture-temperature feedbacks. *Geophys. Res. Lett.* **2017**, *44*, 1511–1519. [[CrossRef](#)]
45. LeComte, D. International Weather Highlights 2013: Super Typhoon Haiyan, Super Heat in Australia and China, a Long Winter in Europe. *Weatherwise* **2014**, *67*, 20–27. [[CrossRef](#)]
46. Luo, M.; Lau, N.C. Heat waves in southern China: Synoptic behavior, long-term change, and urbanization effects. *J. Clim.* **2017**, *30*, 703–720. [[CrossRef](#)]
47. Gu, S.H.; Huang, C.R.; Bai, L.; Chu, C.; Liu, Q.Y. Heat-related illness in China, summer of 2013. *Int. J. Biometeorol.* **2016**, *60*, 131–137. [[CrossRef](#)]
48. Sun, J.; Wang, H.; Yuan, W. Decadal Variability of the Extreme Hot Event in China and Its Association with Atmospheric Circulations. *Clim. Environ. Res.* **2011**, *2*, 199–208.

49. Qian, W.H.; Ding, T. Atmospheric anomaly structures and stability associated with heat wave events in China. *Chin. J. Geophys.* **2012**, *55*, 1487–1500.
50. Zhang, Y.X.; Zhang, S.J. Causation Analysis on a Large -Scale Continuous High Temperature Process Occurring in North China Plain. *Meteorol. Mon.* **2010**, *36*, 8–13.
51. Li, Y.; Ma, B.S.; Yang, X.; Zhang, J.Y. Characteristics of summer heat waves in China Mainland and the relationship between Eastern-/Central-Pacific El Nino and heat wave events. *J. Lanzhou Univ. Nat. Sci.* **2018**, *54*, 711–721.
52. Wang, L.W.; Zhang, J. Relationship Between summer heat waves and soil moisture in North-East China. *J. Meteorol. Sci.* **2015**, *35*, 558–564.
53. Zhang, W.L.; Zhang, J.Y.; Fan, G.Z. Dominant modes of dry- and wet-season precipitation in southwestern China. *Chin. J. Atmos. Sci.* **2014**, *38*, 590–602.



© 2019 by the authors. Licensee MDPI, Basel, Switzerland. This article is an open access article distributed under the terms and conditions of the Creative Commons Attribution (CC BY) license (<http://creativecommons.org/licenses/by/4.0/>).